



# A calibration technique to improve accuracy of the photogrammetry-based deformation measurement method for triaxial testing

Lin Li<sup>1</sup> · Yi Lu<sup>1</sup> · Yang Cai<sup>1</sup> · Peng Li<sup>2</sup>

Received: 26 January 2020 / Accepted: 12 September 2020 / Published online: 25 September 2020  
© Springer-Verlag GmbH Germany, part of Springer Nature 2020

## Abstract

In 2015, a photogrammetry-based method was developed to measure soil deformation during triaxial testing with help of a handheld camera. Since this development, the photogrammetry-based method has been well-recognized due to its simplicity, low cost, and full-field deformation measurement capability. For better characterization of soil deformation during triaxial testing, a simple technique is presented to further improve the accuracy of the photogrammetry-based method through a calibration of four system parameters (i.e., cell wall thickness, refractive index of air, cell wall, and confining media). To evaluate this technique, several tests were performed on a  $61 \times 122$  mm stainless-steel cylinder inside of a  $152 \times 200$  mm triaxial cell. Measurement results indicate that the average point measurement accuracy of the photogrammetry-based was improved to 0.032 mm from 0.081 mm when the triaxial cell used was filled with water.

**Keywords** Optical ray tracing · Photogrammetry-based method · Triaxial test

## 1 Introduction

Both saturated and unsaturated soil triaxial tests require soil volume measurement during testing. The measurement of the unsaturated soil volume/deformation during triaxial testing used to be a great challenge for researchers. In the past, a great deal of research effort has been dedicated to developing different methods such as the double-wall cell (e.g. [3, 19]), local displacement transducers (e.g., [5, 6, 11]), laser [24], and volume controllers (e.g. [4, 13]) for soil volume/deformation measurement during triaxial testing. However, as summarized in Laloui et al. [12] and Zhang et al. [28], all of these methods have their limitations and accurate unsaturated soil deformation measurement during triaxial testing remained a great challenge for researchers.

In 2015, a photogrammetry-based method was developed as presented in Zhang et al. [28] and Li et al. [16] and

later successfully applied for unsaturated soil deformation measurement during triaxial testing as reported in Li and Zhang [14]. With this method, using a conventional saturated soil triaxial testing system, the unsaturated soil volume/deformation during testing can be easily measured with help of a handheld camera. Since this development, the photogrammetry-based method has been well-recognized for its simplicity, low cost, and full-field deformation measurement capability. The newly developed photogrammetry-based method overcomes most of the limitations associated with the other image-based methods (e.g. [1, 2, 8, 17, 18, 21, 26]). With the photogrammetry-based method, the conventional saturated soil triaxial testing system can be used to characterize unsaturated soils without any modification for deformation measurement. Furthermore, the full-field soil deformation measurement capability allows more advanced soil deformation characterization such as volumetric strain non-uniformity, strain localization, 3D bulging, and shear plane evolution of soils during triaxial testing.

In addition to the overall soil volume change, recent findings presented in Alshibli et al. [1], Rechenmacher and Saab [20], Desrues and Viggiani [7], and Rechenmacher [21] revealed that the localized deformation also played important role in soil mechanical behavior. Sachan and

✉ Lin Li  
lli2018@njfu.edu.cn

<sup>1</sup> College of Civil Engineering, Nanjing Forestry University, No. 159 Longpan Road, Nanjing 210037, Jiangsu, China

<sup>2</sup> School of Highway, Chang'an University, Xi'an 710064, Shaanxi, China

Penumadu [25] stated that the strain localization was a major factor which controlled the overall mechanical response of soil, at or near failure. In view of this, significant research effort has been dedicated to characterizing the localized soil deformation during triaxial testing (e.g. [2, 10, 16, 17, 21, 22, 25, 27]). With the photogrammetry-based method, localized strain can be easily extracted from the full-field soil deformation. For the conventional volume change measurement, there is no specific requirement on the point measurement accuracy as long as the overall volume measurement accuracy is within 0.25% [9]. However, different from the volume change measurement, the requirement on the point measurement accuracy is much higher for accurate characterization of strain localization. This is because of strain is interpolated based on the movement of each point on soil surface. As a result, high point measurement accuracy is essential and critical for strain localization and more advanced soil behavior characterization.

Preliminary triaxial test results, as presented in Li et al. [16], and Li and Zhang [14, 15] revealed that the measurement accuracy of the photogrammetry-based method is dependent on several factors such as camera, camera calibration, number of images, assumptions on triaxial cell wall, setup of the measurement targets, and confining media. This measurement accuracy can be improved through using a suitable camera with an accurate calibration, more images, appropriate measurement target setup, and transparent confining fluid with a high refractive index. However, the measurement accuracy of the photogrammetry-based method is still well below that of the photogrammetric method. A simple technique is presented in this study to further improve the accuracy of the photogrammetry-based method through a calibration of four system parameters (i.e. cell wall thickness, refractive index of air, cell wall, and confining media). To evaluate the proposed technique, several tests were performed on a stainless-steel cylinder with/without triaxial cell and with triaxial cell under different confining media conditions. A comparison was then made between the photogrammetric and photogrammetry-based methods to find out the four best-fit system parameters which could lead to the highest measurement accuracy.

## 2 Tests on stainless-steel cylinder

### 2.1 Camera calibration

The camera used for image capturing was Nikon D7500 with a fixed focal length lens (i.e., AF-S Nikkor 50 mm f/1.4G). Before the photogrammetry-based measurement, the camera was calibrated and the result is shown in

**Table 1** Camera calibration result

Parameter	Before idealization	After idealization
$f$ (mm)	54.9184	54.9184
$M$ (pixel)	5568	5568
$N$ (pixel)	3712	3712
$F_x$ (mm)	23.9954	24.3649
$F_y$ (mm)	16.0000	16.2418
$P_x$ (mm)	12.0338	12.1824
$P_y$ (mm)	7.9991	8.1209
$K_1$ ( $10^{-5}$ )	6.264	0
$K_2$ ( $10^{-8}$ )	- 1.257	0
$P_1$ ( $10^{-6}$ )	0	0
$P_2$ ( $10^{-6}$ )	0	0

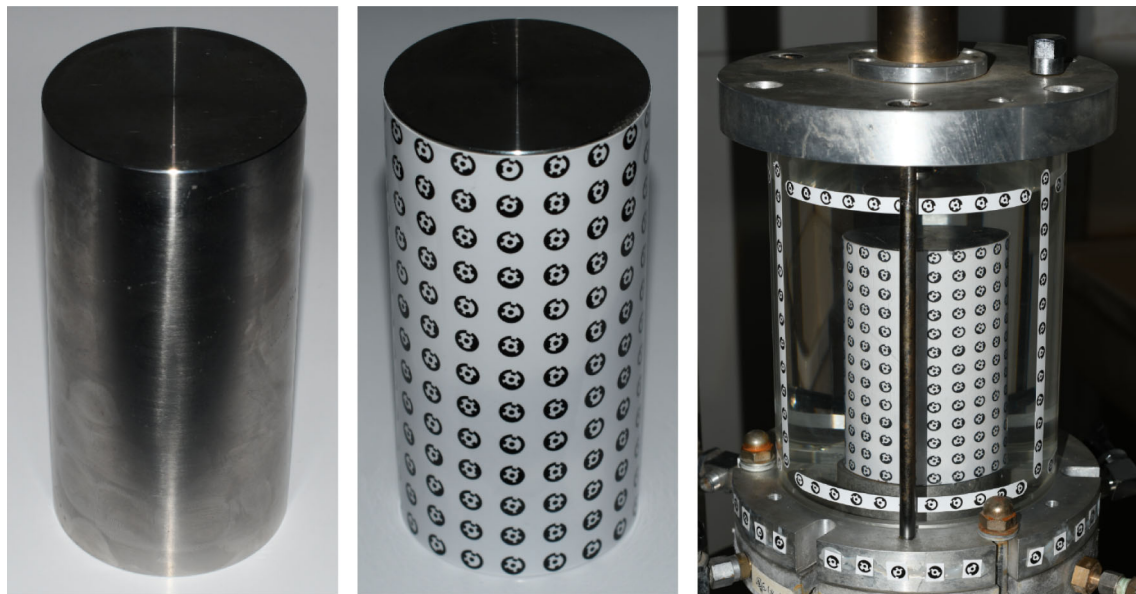
Table 1. The idealized parameters as listed in Column 3 were used for the construction of light rays required by the ray tracing process in the photogrammetry-based method.

### 2.2 Specimen preparation and triaxial testing

A stainless-steel cylinder (i.e. 61 mm in diameter and 122 mm in height, which is consistent with the size of a typical triaxial soil specimen), as shown in Fig. 1a, was fabricated to evaluate the point measurement accuracy of the photogrammetry-based method. A total number of 234 measurement targets (18 targets/circle  $\times$  13 circles) were posted to the cylinder surface, as shown in Fig. 1b, to facilitate the measurements and following accuracy evaluation. The acrylic cell for the triaxial test apparatus, as shown in Fig. 1c, was 200 mm in height, 150 mm in outer diameter with a refractive index of 1.49.

The thickness of the triaxial cell wall was determined to be 10.174 mm through measurements made at two ends using a digital caliper as shown in Fig. 2. The thickness of the cell wall was not uniform. To be specific, at the top end, the thickness of the cell wall varied from 9.82 mm at 6:00 direction to 10.52 mm at 1:00 direction which indicated the maximum difference of 0.70 mm. A similar thickness variation was also found at the bottom end. A total number of 105 measurement targets (in two circles (33 targets/circle) and three vertical stripes (13 targets/strip)), which would be used to locate the camera stations through photogrammetric analyses and reconstruct the cell wall, were posted to the outer surface of the acrylic cell.

The experimental program for the system parameter calibration included measuring the 3D positions of measurement targets on the stainless-steel cylinder surface using the triaxial cell under the following conditions: (1) exposed in the atmosphere; (2) installed in the triaxial cell without any confining fluid; and (3) installed in the triaxial



(a) Stainless-steel cylinder; (b) Cylinder covered with targets; (c) Cylinder in triaxial cell

Fig. 1 Triaxial test setup

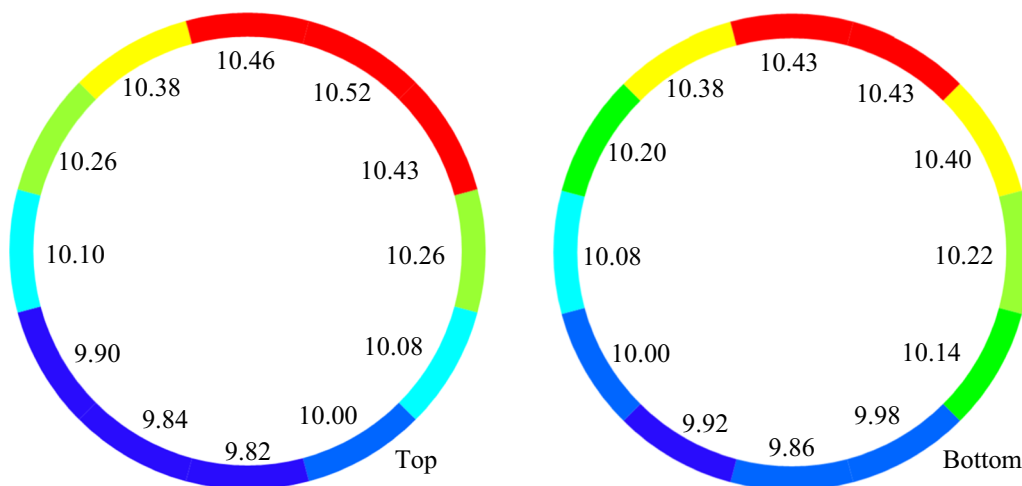


Fig. 2 Cell wall thickness variation (mm)

cell with confining fluid. The 3D coordinates of the measurement targets on cylinder surface measured using the photogrammetric technique before the installation of the triaxial cell provided a reference for measurement accuracy evaluation. The tests were performed according to the following procedure: (1) firmly fix the stainless-steel cylinder on the pedestal of the triaxial cell; (2) capture images to extract the 3D position of the targets on the cylinder surface; (3) carefully install the triaxial cell and capture images for photogrammetry-based measurement; (4) fill the chamber with water and capture images for photogrammetry-based measurement; (5) drain water out, carefully remove the triaxial cell, and then capture images

to extract the 3D position of the targets on the cylinder surface using the photogrammetric method to check if there was any movement of the cylinder during testing.

### 3 Test results

With the help of a software package for photogrammetric analysis, a 3D Cartesian coordinate system was established to facilitate the measurement and accuracy evaluation followed. In this coordinate system, the  $x$ - $y$  plane was parallel to the top and bottom surfaces of the stainless-steel cylinder, the  $z$  direction was set to be the same as the axial

direction of the cylinder, and the center of the coordinate system was set to be at the center of the pedestal top surface. With the images captured, a photogrammetric analysis was performed to reconstruct the triaxial cell surface and the camera stations. Optical rays from each camera station to the targets on specimen surface were then reconstructed using the photogrammetry-based method. To facilitate this reconstruction, four system parameters (i.e., refractive indices of air, cell, and water, cell wall thickness) were respectively set to be 1.000, 1.491, 1.339, and 10.174 mm. Using the targets in the top row on specimen surface (see Fig. 1b) as an example, Fig. 3 shows the top view of the optical rays reconstructed using the photogrammetry-based method for the measurement when the triaxial chamber was filled with water. Two red circles represent the inner and outer surfaces of the triaxial cell wall. For some of the camera stations (e.g.  $CS_1$ ,  $CS_{11}$ , and  $CS_{22}$ ), the number of optical rays reconstructed were much less than that from other camera stations. This was because of the view to the specimen surface was blocked by the targets on cell surface and three tie rods as typically shown in Fig. 1c. According to the enlargement as shown in Fig. 3, an average number of seven optical rays were reconstructed to measure the 3D coordinate of each target.

To measure the 3D coordinate of all targets on cylinder surface, a total number of 1570 optical rays were constructed from different camera stations to the targets on cylinder surface. With the optical rays constructed as typically shown in Fig. 3, a least square estimation was then performed to best estimate the 3D coordinate of each target. A point-by-point comparison was then made between the results from the photogrammetric (i.e., exposed in the atmosphere condition) and photogrammetry-based (i.e., inside of the triaxial chamber with and without water as the

confining media) methods as shown in Fig. 4. Before system parameter calibration, average point measurement errors of 0.141 mm and 0.081 mm were computed respectively for the air-filled and water-filled chamber conditions. The point measurement error for the air-filled chamber condition is much higher than the water-filled condition which is consistent with the finding presented in Li and Zhang [15]. It is interesting to find out that the photogrammetry-based method tended to underestimate the  $y$  value of the target coordinates before filling the chamber with water. After filling the chamber with water, the measurement error was nearly symmetrically along the radial direction of the cylinder which indicated that one or more of four system parameters adopted by the photogrammetry-based method were not accurate.

#### 4 System parameter calibration

With the images captured for the exposed in the atmosphere before and after the measurement with the triaxial cell on, a photogrammetric analysis was performed and the 3D coordinate of the targets on cylinder surface was determined. Through a point-by-point comparison, the average measurement error was determined to be 0.02 mm and the direction of corresponding displacement vectors was arbitrary. Thus, it's reasonable to assume that there was no movement of the cylinder during testing. Consequently, the point measurement error for the cylinder inside of the cell was attributed to the presence of cell wall and confining media. With the measurement results from the above-mentioned tests, a comparison was made between the 3D coordinates of the targets measured in the atmosphere and in the triaxial chamber with confining media

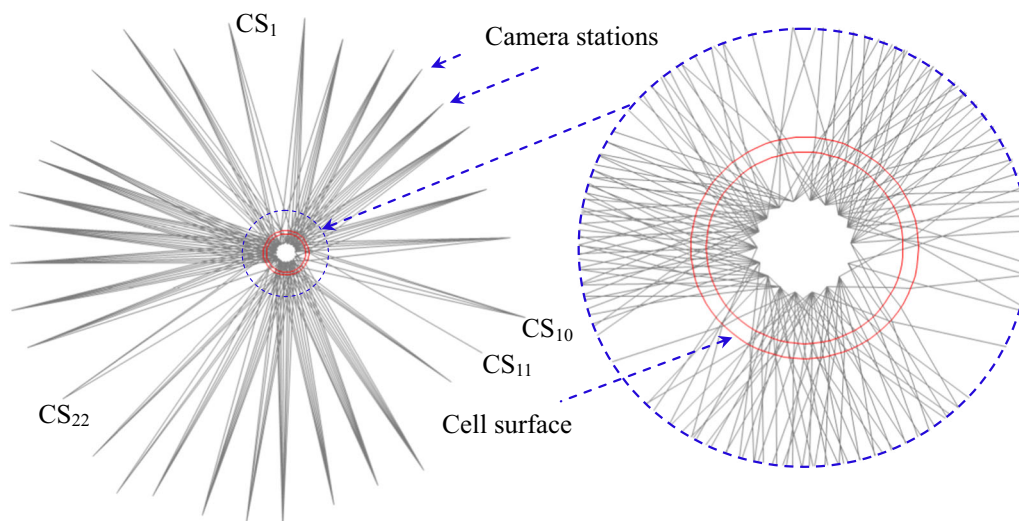


**Fig. 3** Optical rays from different camera stations to targets at the cylinder surface

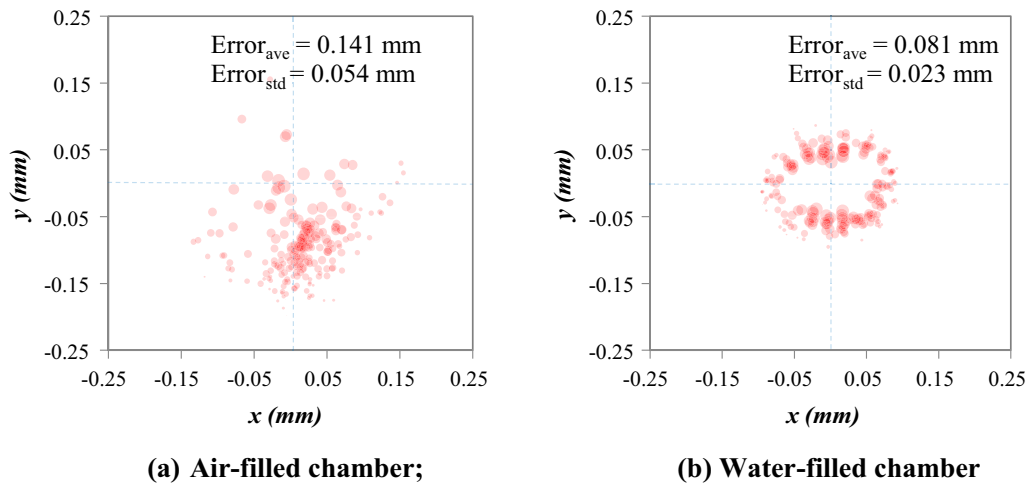


**Fig. 4** Point measurement error distribution before system parameter calibration

condition. Figure 5a, b, respectively, shows the measurement error distribution with different refractive indices of water and air.

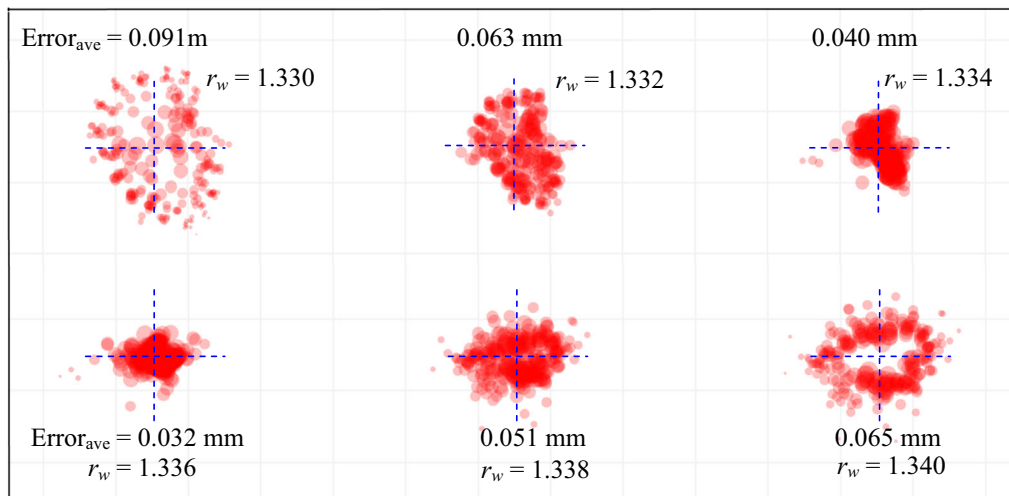
In Fig. 5a, when the refractive index of water increased from 1.33 to 1.34, the average measurement error quickly reduced from 0.091 mm to the minimum value of 0.032 mm at a refractive index of 1.336 and then increased to 0.065 mm. At a refractive index of 1.34, the measurement error is nearly symmetrically distributed along the radial direction of the cylinder. Figure 5c, d, respectively, show the variation of measurement error with different cell wall refractive index and thickness. Similar to the influence of water and air refractive indices, the measurement error decreased to the minimum value and then increased with increasing cell wall refractive index and thickness. According to the calibration results presented in Fig. 5, when the refractive indices of water, air, cell wall, and thickness of cell wall were, respectively, 1.336, 1.0012, 1.494, and 10.32 mm, the average measurement error reached the minimum value of 0.032 mm which was much lower than 0.081 mm before the system parameter calibration.

In the triaxial test on the stainless-steel cylinder performed in this study, a total number of 24 images were used for the measurement. Figure 6a illustrates the image number used for the 3D coordinate estimation of each target. The image number used for the measurement of each target varied from three to nine. The measurement accuracy at each target is plotted in Fig. 6b. The measurement error for the 234 targets on cylinder surface was within 0.12 mm. High measurement error zone is found to be at the lower end. The high measurement error in this zone is likely attributed to the variation in cell wall thickness since the corresponding image numbers are relatively high. Figure 6c presents the measurement error

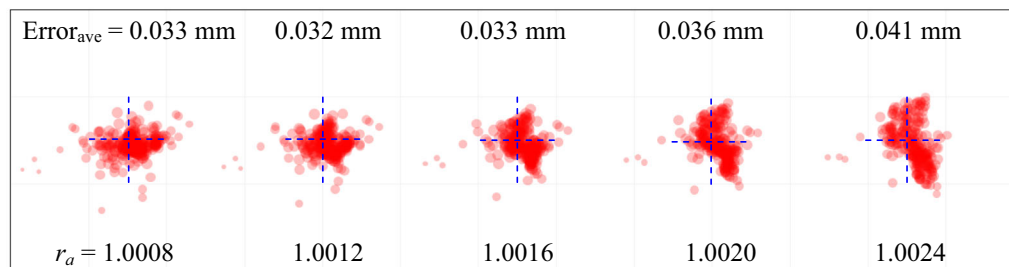
versus the number of images used for each target. A linear regression analysis indicated that the point measurement error insignificantly decreased with increasing number of images. As a result, improving the measurement accuracy through increasing the number of images for the photogrammetry-based analysis may not be a wise option especially when the time required to processing those extra images are taken into consideration. Figure 6d shows the measurement error (i.e. distance between the target position measured using the photogrammetric method before the installation of the triaxial cell to the corresponding optical ray) versus the incident angle of each optical ray (1570 rays in total) before the refraction at the air-cell interface. A lower incident angle is beneficial in reducing the measurement error according to the linear regression result. However, this influence of incident angle on the point measurement accuracy is also insignificant. As a result, the image capturing can be made at any arbitrary angle without compromising the measurement accuracy.

## 5 Discussions

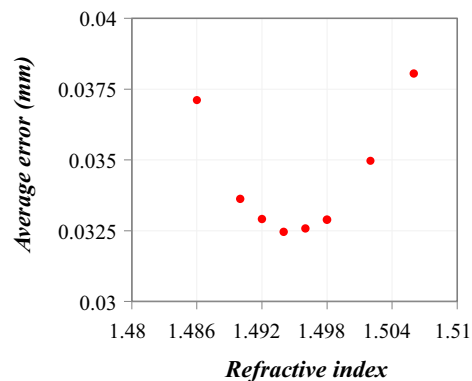
As addressed before, four system parameters are required to be calibrated to improve the accuracy of the photogrammetry-based method. According to the results presented in this study, the refractive index of the confining media is the most critical parameter which can significantly influence the accuracy of the photogrammetry-based method. Among four parameters, the calibration on the refractive index of the confining media should be made first. Otherwise, the influence of other parameters can be largely shaded due to an inaccurate confining media refractive index which can possibly lead to an inaccurate estimation of the other system parameters.



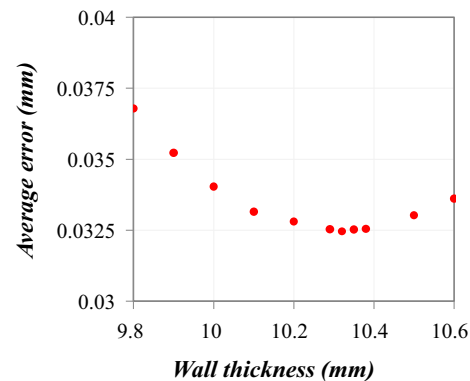
(a) Water refractive index calibration;



(b) Air refractive index calibration;



(c) Cell refractive index calibration;



(d) Cell thickness calibration

Fig. 5 System parameter calibration

It should be mentioned that the parameters calibrated may be slightly different from the measurement values. For example, the cell wall thickness used in the photogrammetry-based method is 10.320 mm instead of 10.174 mm which was the average thickness of the cell wall measured using a digital caliper. As a result, in terms of better measurement accuracy, system parameters obtained through direct measurement may not be the best for the photogrammetry-based method.

According to Richerzhagen [23], besides light wavelength, the refractive index of water is also dependent on temperature. Consequently, the system setup for the calibration test should be consistent with the triaxial testing on soil specimens. To be specific, the same triaxial cell, camera, lighting condition, confining fluid, and testing temperature are recommended to be the same. For testing using a new triaxial system, the calibration process for the system parameters is strongly suggested for better measurement accuracy.

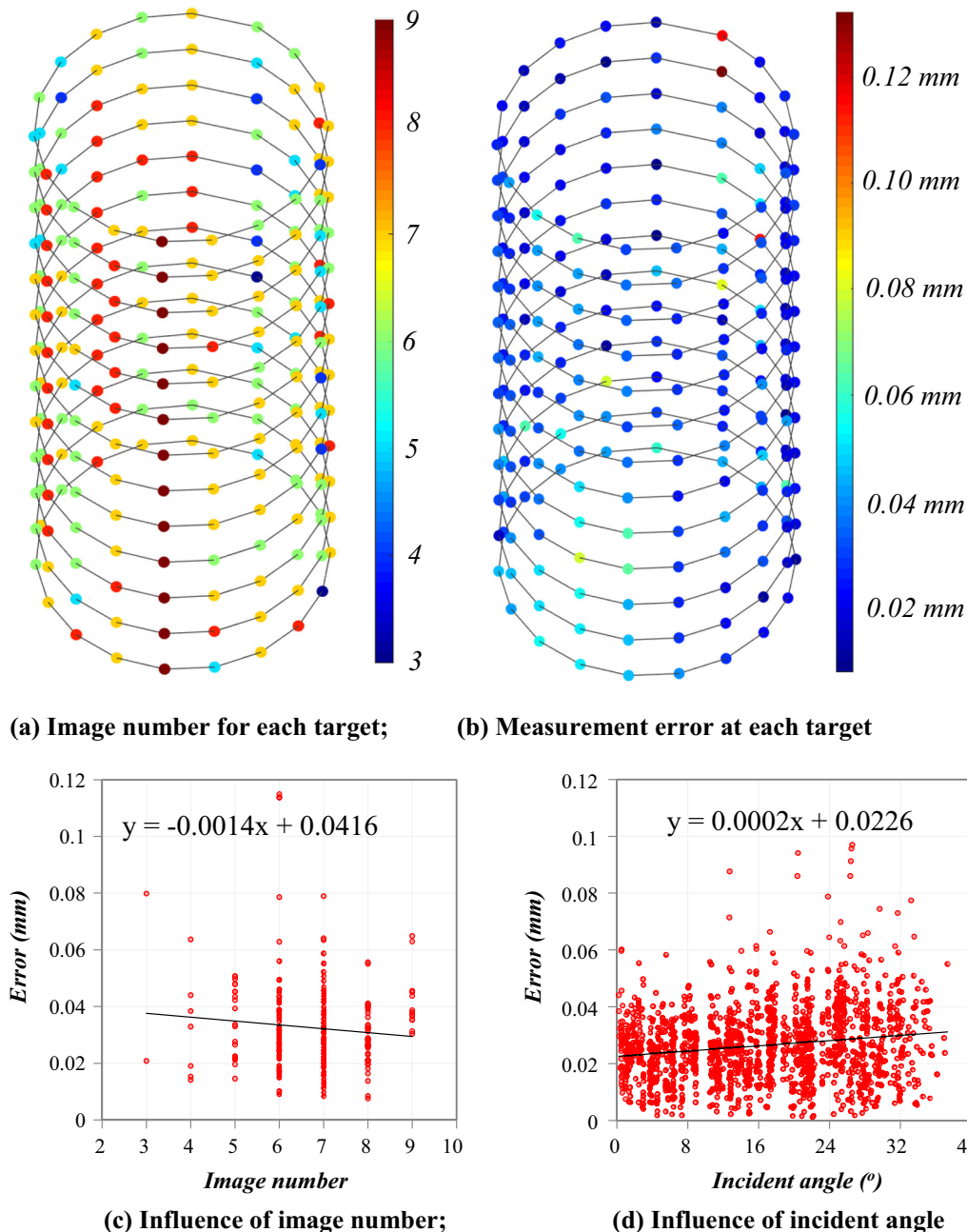


Fig. 6 Measurement error analysis

## 6 Conclusions

This study proposed a simple technique to calibrate the system parameters required for the photogrammetry-based method through triaxial testing on a stainless-steel cylinder. The refractive index of the confining fluid, which is the most critical parameter, is calibrated first to eliminate the influence of inaccurate refractive index of confining media on other parameters. The calibrations for the cell wall thickness, refractive indices of air and cell wall were performed thereafter. With this calibration technique, direct

measurement of four system parameters is no longer required. Most importantly, the average point measurement accuracy of the photogrammetry-based method is significantly improved from 0.081 mm to 0.032 mm with the proposed calibration technique.

**Acknowledgements** This work is supported by the National Natural Science Foundation of China (Grant No. 51709088).

## References

- Alshibli KA, Sture S, Costes NC, Lankton ML, Batiste SN, Swanson RA (2000) Assessment of localized deformations in sand using X-ray computed tomography. *Geotech Test J* 23(3):274–299. <https://doi.org/10.1007/s100100000044>
- Bhandari AR, Powrie W, Harkness RM (2012) A digital image-based deformation measurement system for triaxial tests. *Geotech Test J* 35(2):209–226. <https://doi.org/10.1520/gtj103821>
- Bishop AW, Donald IB (1961) The experimental study of partly saturated soil in the triaxial apparatus. In: Proceedings of 5th international conference of soil mechanics, vol 1, pp 13–21
- Cabarkapa Z, Cuccovillo T (2006) Automated triaxial apparatus for testing unsaturated soils. *Geotech Test J* 29(1):21–29. <https://doi.org/10.1520/gtj12310>
- Clayton CR, Khatrush SA, Bica AV, Siddique A (1989) Hall effect sensors in geotechnical instrumentation. *Geotech Test J* 12(1):69–76
- Cuccovillo T, Coop MR (1997) The measurement of local axial strains in triaxial tests using LVDTs. *Geotechnique* 47(1):167–171. <https://doi.org/10.1680/geot.1997.47.1.167>
- Desrues J, Viggiani G (2004) Strain localization in sand: an overview of the experimental results obtained in Grenoble using stereophotogrammetry. *Int J Numer Anal Methods Geomech* 28(4):279–321. <https://doi.org/10.1002/nag.338>
- Gachet P, Klubertanz G, Vulliet L, Laloui L (2003) Interfacial behavior of unsaturated soil with small-scale models and use of image processing techniques. *Geotech Test J* 26(1):12–21. <https://doi.org/10.1520/GTJ11099J>
- GDS Instruments (2009). [http://www.gdsinstruments.com/\\_assets\\_/products/000013/UNSAT\\_Datasheet.pdf](http://www.gdsinstruments.com/_assets_/products/000013/UNSAT_Datasheet.pdf). Last accessed 28 Dec 2019
- Ji X, Kong X, Zou D, Sang Y, Zhou C, Liu J, Zhao J (2020) Measurement of membrane penetration in triaxial specimen through digital image correlation. *Acta Geotech*. <https://doi.org/10.1007/s11440-020-00998-6>
- Knittel L, Wichtmann T, Niemunis A, Huber G, Triantafyllidis T (2020) Pure elastic stiffness of sand represented by response envelopes derived from cyclic triaxial tests with local strain measurements. *Acta Geotech*. <https://doi.org/10.1007/s11440-019-00893-9>
- Laloui L, Peron H, Geiser F, Rifa'i A, Vulliet L (2006) Advances in volume measurement in unsaturated triaxial tests. *Soils Found* 46(3):341–349. <https://doi.org/10.3208/sandf.46.341>
- Laudahn A, Sosna K, Bohdp J (2005) A simple method for air volume change measurement in triaxial tests. *Geotech Test J* 28(3):313–318. <https://doi.org/10.1520/GTJ12656>
- Li L, Zhang X (2015) A new triaxial testing system for unsaturated soil characterization. *Geotech Test J* 38(6):823–839. <https://doi.org/10.1520/gtj20140201>
- Li L, Zhang X (2019) Factors influencing the accuracy of the photogrammetry-based deformation measurement method. *Acta Geotech* 14(2):559–574. <https://doi.org/10.1007/s11440-018-0663-4>
- Li L, Zhang X, Chen G, Lytton R (2015) Measuring unsaturated soil deformations during triaxial testing using a photogrammetry-based method. *Can Geotech J* 53(3):472–489. <https://doi.org/10.1139/cgj-2015-0038>
- Lin H, Penumadu D (2006) Strain localization in combined axial torsional testing on kaolin clay. *J Eng Mech* 132(5):555–564. [https://doi.org/10.1061/\(ASCE\)0733-9399\(2006\)132:5\(555\)](https://doi.org/10.1061/(ASCE)0733-9399(2006)132:5(555))
- Macari EJ, Parker JK, Costes NC (1997) Measurement of volume changes in triaxial tests using digital imaging techniques. *Geotech Test J* 20(1):103–109. <https://doi.org/10.1520/GTJ11424J>
- Ng CW, Zhan LT, Cui YJ (2002) A new simple system for measuring volume changes in unsaturated soils. *Can Geotech J* 39(3):757–764. <https://doi.org/10.1139/t02-015>
- Rechenmacher A, Saab N (2002) Digital image correlation (DIC) to evaluate progression and uniformity of shear bands in dilative sands. In: 15th ASCE engineering mechanics conference, Columbia University, NY, June 5th
- Rechenmacher AL (2006) Grain-scale processes governing shear band initiation and evolution in sands. *J Mech Phys Solids* 54:22–45. <https://doi.org/10.1016/j.jmps.2005.08.009>
- Rechenmacher AL, Medina-Cetina Z (2007) Calibration of soil constitutive models with spatially varying parameters. *J Geotech Geo-environ Eng* 133(12):1567–1576. [https://doi.org/10.1061/\(ASCE\)1090-0241\(2007\)133:12\(1567\)](https://doi.org/10.1061/(ASCE)1090-0241(2007)133:12(1567))
- Richerzhagen B (1996) Interferometer for measuring the absolute refractive index of liquid water as a function of temperature at 1.064  $\mu\text{m}$ . *Appl Opt* 35(10):1650–1653. <https://doi.org/10.1364/AO.35.001650>
- Romero E, Facio JA, Lloret A, Gens A, Alonso EE (1997) A new suction and temperature controlled triaxial apparatus. In: Proceedings of the 14th international conference on soil mechanics and foundation engineering, Hamburg, vol 1, pp 185–188
- Sachan A, Penumadu D (2007) Strain localization in solid cylindrical clay specimens using digital image analysis (DIA) technique. *Soils Found* 47(1):67–78. <https://doi.org/10.3208/sandf.47.67>
- Salazar SE, Coffman RA (2015) Consideration of internal board camera optics for triaxial testing applications. *Geotech Test J* 38(1):40–49. <https://doi.org/10.1520/GTJ20140163>
- Wang P, Guo X, Sang Y, Shao L, Yin Z, Wang Y (2020) Measurement of local and volumetric deformation in geotechnical triaxial testing using 3D-digital image correlation and a subpixel edge detection algorithm. *Acta Geotech*. <https://doi.org/10.1007/s11440-020-00975-z>
- Zhang X, Li L, Chen G, Lytton R (2015) A photogrammetry-based method to measure total and local volume changes of unsaturated soils during triaxial testing. *Acta Geotech* 10(1):55–82. <https://doi.org/10.1007/s11440-014-0346-8>

**Publisher's Note** Springer Nature remains neutral with regard to jurisdictional claims in published maps and institutional affiliations.